AIAA-98-0029

AEROELASTIC BEHAVIOR OF TWIST-COUPLED HAWT BLADES

Don W. Lobitz and Paul S. Veers
Sandia National Laboratories
Albuquerque, New Mexico 87185-0439

Abstract

As the technology for HAWT development matures, more novel techniques are required for the capture of additional amounts of energy, alleviation of loads and control of the rotor. One such technique employs the use of an adaptive blade that could sense the wind velocity or rotational speed in some fashion and accordingly modify its aerodynamic configuration to meet a desired objective. This could be achieved in either an active or passive manner, although the passive approach is much more attractive due to its simplicity and economy. As an example, a blade design might employ coupling between bending and/or extension, and twisting so that, as it bends and extends due to the action of the aerodynamic and inertial loads, it also twists modifying the aerodynamic performance in some way. These performance modifications also have associated aeroelastic effects, including effects on aeroelastic instability. These aeroelastic effects are the topic of this paper. To address the scope and magnitude of these effects a tool has been developed for investigating classical flutter and divergence of HAWT blades. As a starting point, an adaptive version of the uniform Combined Experiment Blade will be investigated. Flutter and divergence airspeeds will be reported as a function of the strength of the coupling, and also be compared to those of generic blade counterparts.

Background

There have been many efforts aimed at creating adaptive blades using material elastic coupling to replace mechanical devices with passive techniques. Several have used the composite lay-up structure to create a coupling between the twisting of the blade (directly affecting angle of attack) and various other inherent forces. Karaolis[1,2] illustrates how to achieve power control with such a blade on a small system and even provides optimum composite ply structures to provide maximum coupling. Joose and van den Berg[3,4] have publicized efforts to develop a special twist/axial coupled spar that will rotate a tip mechanism through large enough angles to control power and provide some over-speed protection. Infield and Feuchtwang[5,6] show how small turbines can have improved speed regulation with twist/axial coupling. A common feature in these works is to provide relatively large rotations to achieve substantial amounts of power regulation. Most have used stretch twist coupling on variable speed systems to assist in over-speed control or power regulation and rely on large angles of twist to accomplish complete control of high wind loads. Lobitz[7], however, demonstrated that even with relatively small twists (that incidentally also enhance regulation), a stall controlled, fixed pitch system could be operated with a larger rotor to achieve net energy enhancements without increasing the maximum power rating.

An excellent report evaluating a great variety of passive methods of achieving power control (Corbet and Morgan, Reference 8) demonstrates how difficult it is to achieve flat power regulation (constant power versus wind speed) in high winds with passive methods alone. The report does not examine aeroelastic tailoring through composite lay-up structure because it is judged too difficult to produce in a reliable manner given current hand-lay-up techniques of blade manufacturing. They infer that manufacturing improvements are needed before aeroelastic tailoring based on material coupling can be fully implemented on utility scale machines.

Here we examine more modest twist angles intended to produce load alleviation and perhaps power regulation or enhancement through bend/twist coupling. It seems quite possible to reduce the rotor dynamic response by enhancing aeroelastic damping in critical modes of vibration. Eggers, et al.[9] have shown how a simple control system, in some ways similar to coupling between root bending and blade pitch, can reduce low frequency blades loads substantially. However, when modifications that influence aeroelastic behavior are introduced into a rotor there is always the possibility of also introducing instabilities. Stability is studied here by mapping out regions of potential coupling, creating a finite element formulation for coupled blades, and evaluating an example blade with added twist coupling. The load alleviating capabilities are not evaluated here but will be the topic of follow-on studies.

This work was supported by the United States Department of Energy, Sandia National Laboratories under Contract DE-AC04-94AL85000.

Introduction

Before the aeroelastic behavior of adaptive blades is studied, an investigation into the limits of the magnitude of the coupling is investigated. Aeroelastic stability computations are then completed within the range of these limits. Two types of aeroelastic instability are investigated, divergence and classical flutter. Divergence is a static phenomenon wherein the flow velocity (due to both the ambient wind speed and the rotor rotation rate) becomes great enough so that the load produced for an incremental angle of attack change due to blade twisting is greater than the reaction load produced by the elastic restoring forces for the same amount of twist. The result is an effective loss of stiffness so the blade twists without bound, leading to catastrophic failure. Classical flutter is a dynamic phenomenon characterized by an interaction between blade bending and twisting oscillations. As the flow velocity increases, the aerodynamic loading causes the vibratory phase between these two motions to change, eventually leading to a negative damping situation and catastrophic failure. Both of these phenomena can occur at low angle of attack. A third type of aeroelastic instability, which will not be addressed in this paper, is stall flutter. It is characterized by predominantly torsional blade oscillation and normally occurs at high angle of attack near stall.

The finite element model used for this study includes centrifugal stiffening of the blades and rotating coordinate system effects in a manner similar to that done in Reference 10. The "tennis racket" effect, wherein the blade tends to flatten into the plane of rotation due to the chordwise distribution of mass loaded by centrifugal forces, is modeled by distributing the blade mass fore and aft along the chord at each node as two equal lumped masses. The masses are equidistant from the node and the distance between them is adjusted so that the correct torsional inertia is obtained. The incorporation of aeroelasticity terms is based on Theodorsen's equations[11] for the lift and moment on an oscillating airfoil in terms of its plunging and pitching motions (bending and twisting for a HAWT blade). The principle of virtual work is employed to cast them into the finite element framework[12]. The MSC NASTRAN commercial finite element code is used for this analysis, incorporating the special effects mentioned above and the special couplings described in the next paragraph through the Direct Matrix Input at Grids (DMIG) input option. Special purpose software computes the necessary matrix input values and generates required data records for the input stream.

Coupling between extension and twist, and bending and twist is implemented in the beam element used to model the HAWT blades and will be discussed in greater detail in the next section. The third section of this paper contains results of the aeroelastic instability study for the bending-twist adaptive blade. Conclusions and recommendations are presented in the last section.

Coupling Terms for Beam Elements

The coupling terms for the beam elements in this analysis are generated starting with beam "stress-strain" relations. Coupling terms are developed for extension-twist coupling and bending-twist coupling, followed by a static demonstration of the bending-twist coupling for the Combined Experiment Blade (CEB).

Extension-Twist Coupling

For the extension-twist coupling the beam "stress-strain" relations at a point are given in matrix form below:

$$\begin{bmatrix} EA & -g \\ -g & GK \end{bmatrix} \begin{bmatrix} \frac{\partial u}{\partial x} \\ \frac{\partial \varphi}{\partial x} \end{bmatrix} = \begin{bmatrix} F \\ M_t \end{bmatrix} \qquad (1)$$

As shown in Figure 1, u is the axial displacement, φ is the axial twist, F is the axial force, M_t is the twisting moment, and K is the geometric torsional stiffness factor (for a circular cross section, K is equal to J, the polar moment of inertia of the cross section). The quantity, g, is the coupling term, which is zero for the standard beam where no coupling is present between extension and twist. In order for this system to be positive definite,

$$|g| < \sqrt{EAGK} \qquad (2)$$

To investigate intermediate values of the coupling term, it is taken to be:

$$g = \alpha\sqrt{EAGK}, \quad -1 < \alpha < 1 \qquad (3)$$

There are, of course, additional bending terms in the beam "stress-strain" relations, but only the above terms impact the development of the coupling term for this type of coupling.

Taking u and φ to vary linearly along the element length and using the principle of virtual work, the finite

element representation of Equation 1 becomes:

$$\frac{1}{l}\begin{bmatrix} EA & -g & -EA & g \\ -g & GK & g & -GK \\ -EA & g & EA & -g \\ g & -GK & -g & GK \end{bmatrix}\begin{bmatrix} u_1 \\ \varphi_1 \\ u_2 \\ \varphi_2 \end{bmatrix} = \begin{bmatrix} F_1 \\ M_{t_1} \\ F_2 \\ M_{t_2} \end{bmatrix} \qquad (4)$$

Here l is the length of the element. For illustrative purposes it is instuctive to examine the behavior of a one element beam. If the "1" end of this element is held fixed, the displacements at the "2" end can be obtained in terms of the applied forces at that end, yielding:

$$\begin{bmatrix} u_2 \\ \varphi_2 \end{bmatrix} = l\begin{bmatrix} \frac{1}{1-\alpha^2}\left(\frac{1}{EA}\right) & \frac{\alpha}{1-\alpha^2}\left(\frac{1}{\sqrt{EAGK}}\right) \\ \frac{\alpha}{1-\alpha^2}\left(\frac{1}{\sqrt{EAGK}}\right) & \frac{1}{1-\alpha^2}\left(\frac{1}{GK}\right) \end{bmatrix}\begin{bmatrix} F_2 \\ M_{t_2} \end{bmatrix} \qquad (5)$$

The coefficients in the matrix involving α [$1/(1-\alpha^2)$ and $\alpha/(1-\alpha^2)$] are plotted in Figure 2. This figure along with Equation 5 indicate how the various forces affect the coupled motion for the extension-twist coupling. From Equation 5, if $F_2>0$ and $M_{t_2}=0$, the extension and the twist are positive.

Extension-Twist Demonstration

To exercise this coupled element, the uniform CEB shown in Figure 1 is modeled. The "tennis racket" effect is modeled as described above by distributing the mass fore and aft as shown and the blade is pitched toward stall $12°$. A small amount of coning ($3.5°$) is apparent in Figure 1. With the rotor turning in still air at 72 rpm (1.2 Hz), the tip rotation and axial extension are shown in Figure 2 as a function of the coupling coefficient. In this figure, positive tip rotation corresponds to twisting toward stall. For this loading condition, at 80% of the available coupling, tip rotations of approximately $1.0°$ towards stall and $0.1°$ toward feather are obtained. Part of the reason for this difference in magnitude is the aeroload differences that occur due to the twisting of the blade (the model includes these aeroelastic effects). The tip axial extension varies between .0019 and .0163 inches, as shown. The tip flapwise deflection (not shown in Figure 2) varies between 2.86 and 3.06 inches. It is anticipated that at least a couple of degrees of twist will be required for effective load alleviation .

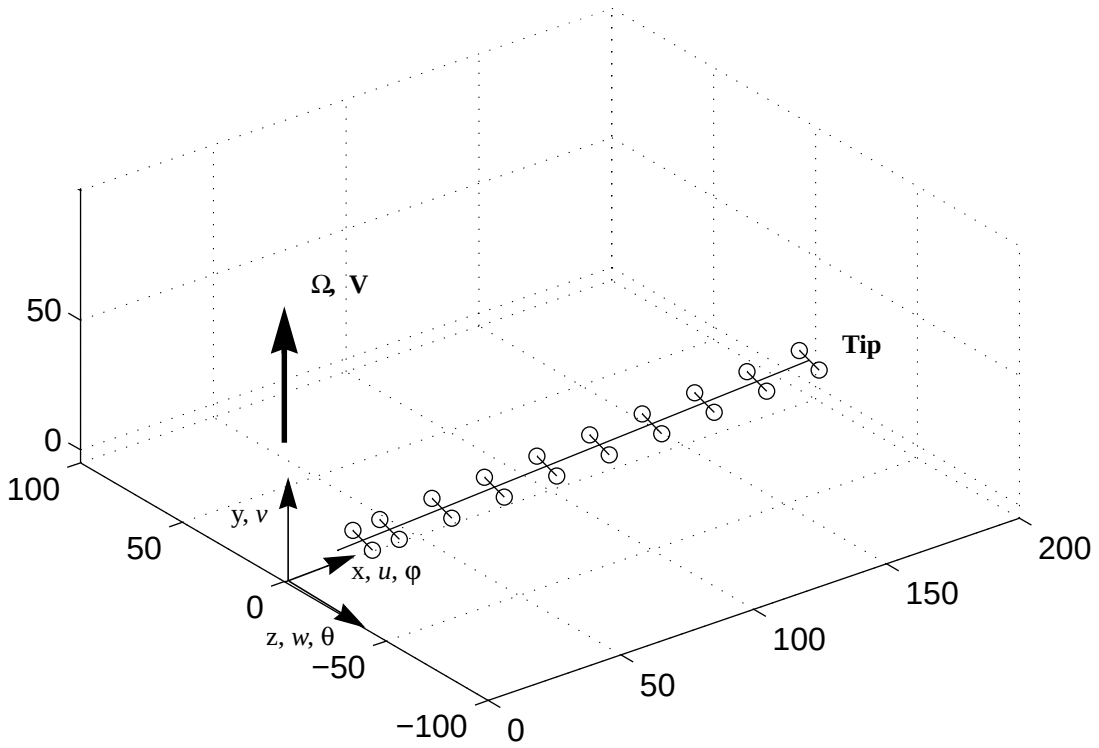

Figure 1. Untwisted Combined Experiment Blade (CEB) Model.

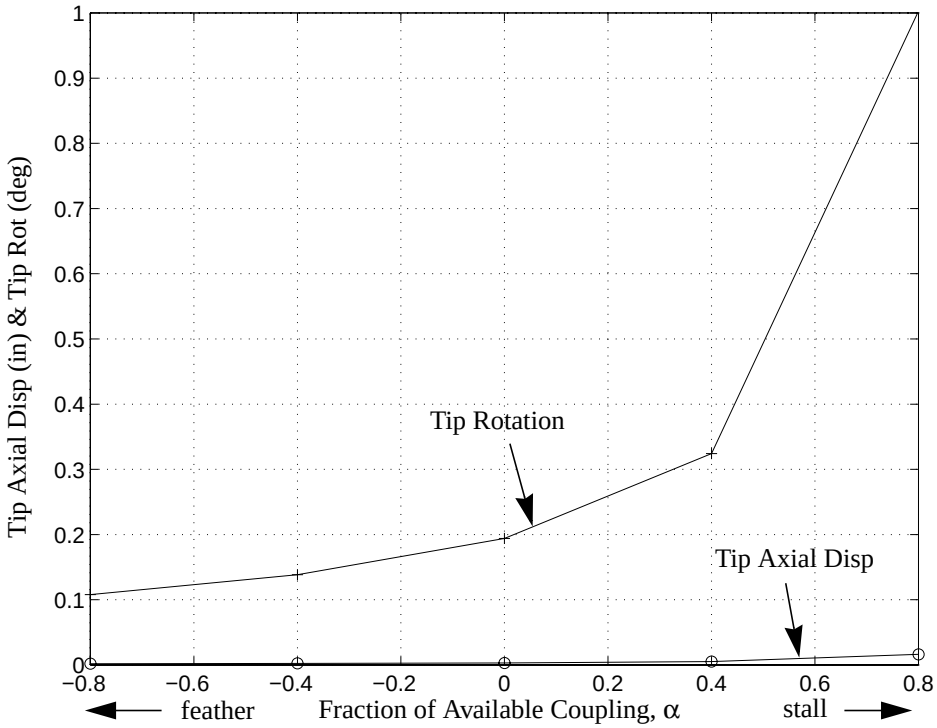

Figure 2. Tip Motion of the Extension-Twist Coupled CEB Turning at 72 rpm in Still Air.

Bending-Twist Coupling

For the bending-twist coupling the "stress strain" relations at a point are given by:

$$\begin{bmatrix} EI & -g \\ -g & GK \end{bmatrix} \begin{bmatrix} \frac{\partial \theta}{\partial x} \\ \frac{\partial \varphi}{\partial x} \end{bmatrix} = \begin{bmatrix} M_b \\ M_t \end{bmatrix} \qquad (6)$$

Referring to Figure 1, $\theta = \partial v / \partial x$ (v is the flapwise displacement) and M_b is the bending moment. In order for this system to be positive definite g is taken to be:

$$g = \alpha\sqrt{EIGK}, \quad -1 < \alpha < 1 \qquad (7)$$

The quantity, α, serves the same function here as in the extension-twist coupling. Only bending in the flapwise direction is accounted for in Equation 6. Bending in the edgewise direction is considered to be small relative to the flapwise direction, yielding minimal coupling. The axial extension term in the beam "stress-strain" relations does not impact this type of coupling.

Taking v to vary quadratically and φ to vary linearly along the element length (a customary practise for beam element development), and using the principle of virtual work, the finite element representation of Equation 6 becomes:

$$\frac{1}{l}\begin{bmatrix} 12EI/l^2 & 6EI/l & 0 & -12EI/l^2 & 6EI/l & 0 \\ 6EI/l & 4EI & -g & -6EI/l & 2EI & g \\ 0 & -g & GK & 0 & g & -GK \\ -12EI/l^2 & -6EI/l & 0 & 12EI/l^2 & -6EI/l & 0 \\ 6EI/l & 2EI & g & -6EI/l & 4EI & -g \\ 0 & g & -GK & 0 & -g & GK \end{bmatrix} \begin{bmatrix} v_1 \\ \theta_1 \\ \varphi_1 \\ v_2 \\ \theta_2 \\ \varphi_2 \end{bmatrix} = \begin{bmatrix} F_1 \\ M_{b_1} \\ M_{t_1} \\ F_2 \\ M_{b_2} \\ M_{t_2} \end{bmatrix}$$

(8)

The quantities, F_1 and F_2 are transverse forces at the ends of the beam element. As before, if the "1" end of this element is held fixed, the displacements at the "2" end can be obtained in terms of the applied forces at that end, yielding:

$$\begin{bmatrix} v_2 \\ \theta_2 \\ \varphi_2 \end{bmatrix} = \begin{bmatrix} \frac{1-(\alpha/2)^2}{1-\alpha^2}\left(\frac{l^3}{3EI}\right) & \frac{1}{1-\alpha^2}\left(\frac{l^2}{2EI}\right) & \frac{\alpha}{1-\alpha^2}\left(\frac{l^2}{2\sqrt{EIGK}}\right) \\ \frac{1}{1-\alpha^2}\left(\frac{l^2}{2EI}\right) & \frac{1}{1-\alpha^2}\left(\frac{l}{EI}\right) & \frac{\alpha}{1-\alpha^2}\left(\frac{l}{\sqrt{EIGK}}\right) \\ \frac{\alpha}{1-\alpha^2}\left(\frac{l^2}{2\sqrt{EIGK}}\right) & \frac{\alpha}{1-\alpha^2}\left(\frac{l}{\sqrt{EIGK}}\right) & \frac{1}{1-\alpha^2}\left(\frac{l}{GK}\right) \end{bmatrix} \begin{bmatrix} F_2 \\ M_{b_2} \\ M_{t_2} \end{bmatrix}$$

(9)

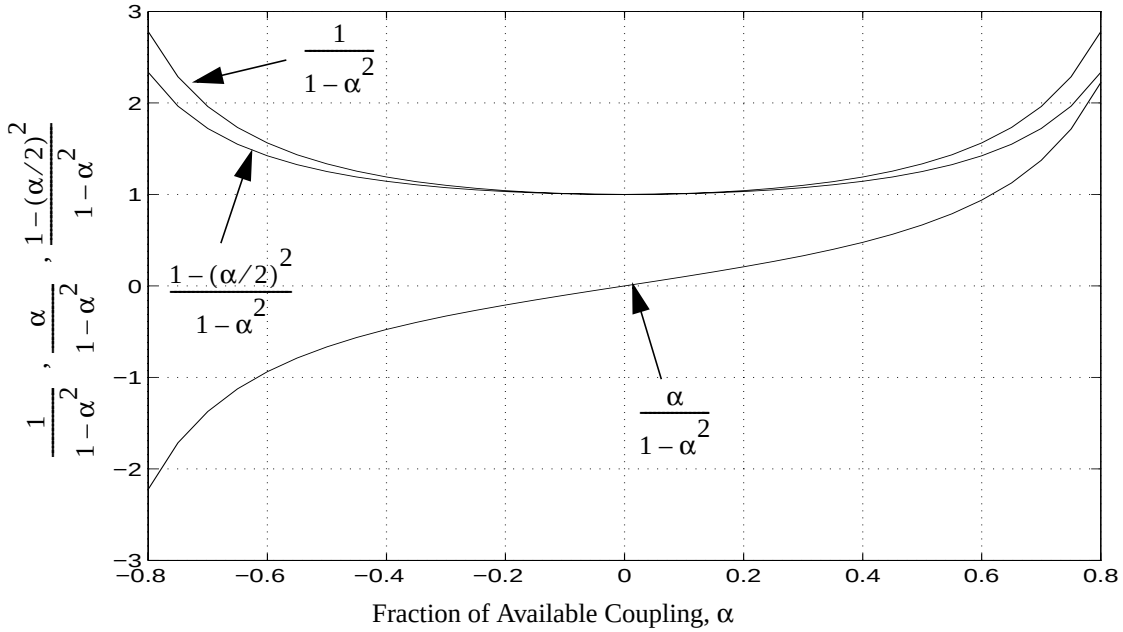

Figure 3. Coefficients of matrix elements involving α.

The coefficients in the matrix of Equation 9 involving α, $1/(1-\alpha^2)$, $\alpha/(1-\alpha^2)$ and $(1-(\alpha/2)^2)/(1-\alpha^2)$, two of which are equivalent to those of Equation 5, are plotted in Figure 3. For $F_2>0$ and $M_{b_2}=M_{t_2}=0$, the flapwise displacement, the slope and the twist are all positive.

Bending-Twist Demonstration

As for the extension-twist element, the uniform CEB shown in Figure 1 is used to exercise the bending-twist element. As before, the "tennis racket" effect is modeled as described by distributing the mass fore and aft as shown and the blade is pitched toward stall $12°$. With the rotor turning in still air at 72 rpm (1.2 Hz), the tip flapwise displacement and axial rotation are shown in Figure 4 as a function of the coupling coefficient. Also shown in Figure 4 is the twist toward feather resulting from the "tennis racket" effect, which, for this relatively stiff blade, is negligible compared to that due to the coupling. In this figure, positive tip rotation corresponds to

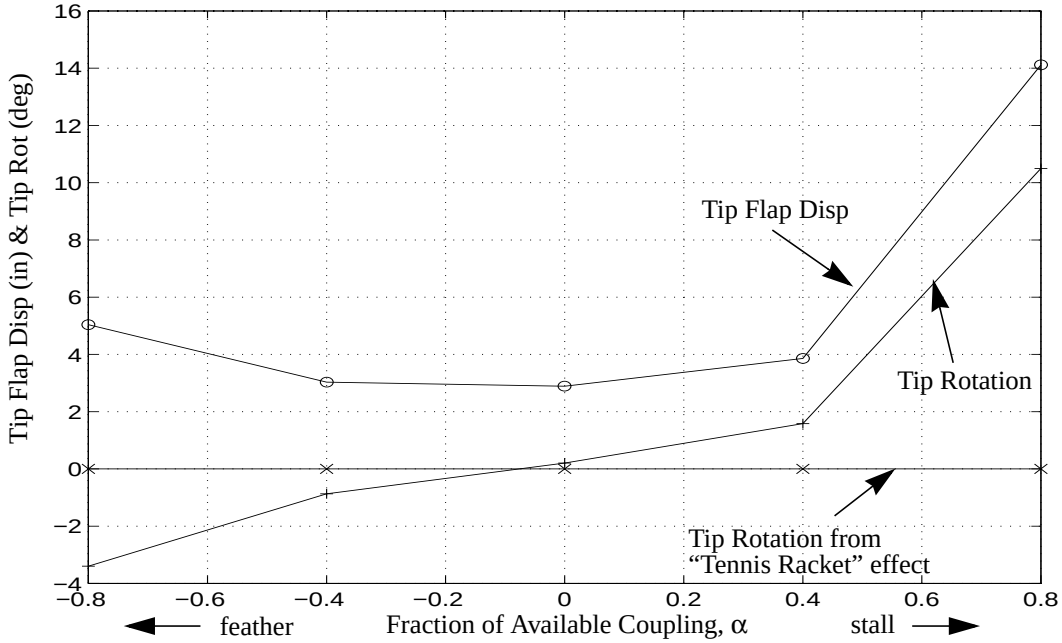

Figure 4. Tip Motion of the Bending-Twist Coupled CEB Turning at 72 rpm in Still Air.

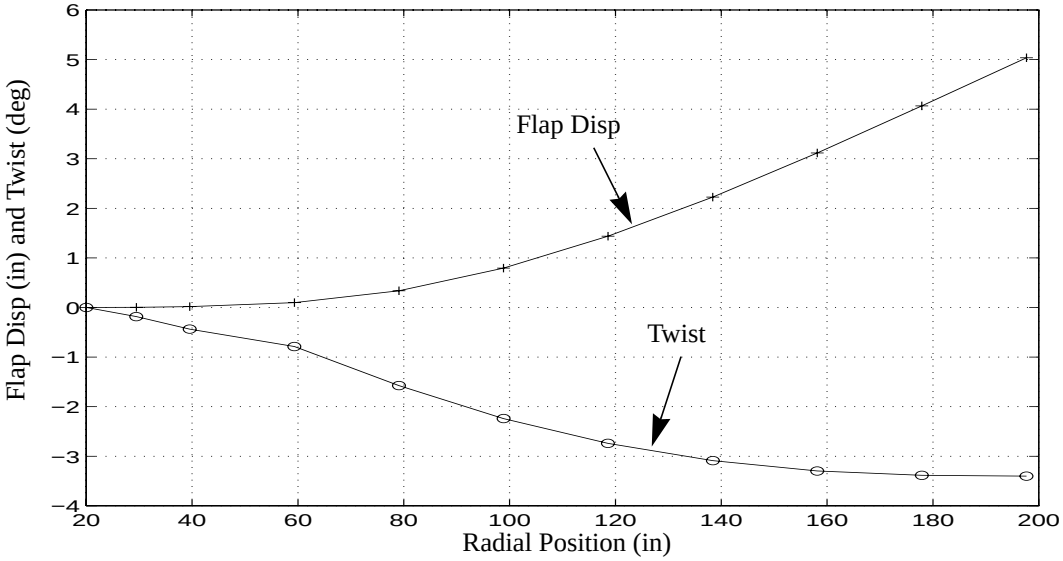

Figure 5. Distribution of Flap Displacement and Twist for the Bending-Twist Coupled CEB.

twisting toward stall. The curves for both the tip displacement and rotation appear to be roughly a linear combination of those ofFigure 3, which is reasonable since the loading consists of a combination of forces, bending moments and twisting moments. For this loading condition, at 80% of the available coupling, tip rotations of approximately 10° towards stall and 3° toward feather are obtained. As before, part of the reason for this difference in magnitude is the aeroload differences that occur due to the twisting of the blade (the model includes these aeroelastic effects). For load alleviation it is anticipated that at least a couple of degrees of twist will be required.

In addition to the tip motions of the blade, the distribution of the motion along the blade is of interest for ascertaining the magnitudes of the total loads on the blade due to the coupling. In Figure 5 , this distribution is shown for the case of α = -0.8. It is apparent for this blade that the coupling produces twist towards feather within 90% of the tip value over the outer third of its span.

In Figure 6 the effect of the coupling on the first flap and torsional natural frequencies (also computed using NASTRAN) is presented. These two modes of vibration have significant impact on the aeroelastic stability

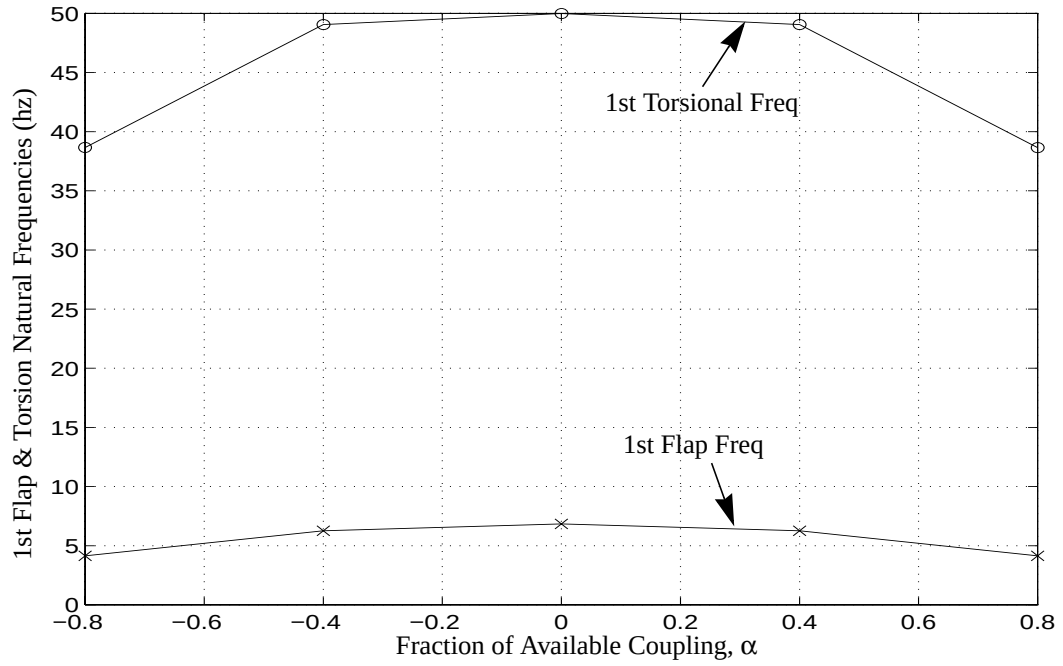

Figure 6. Natural Frequencies of the 1st Torsional and Flap Modes Versus Coupling Coefficient.

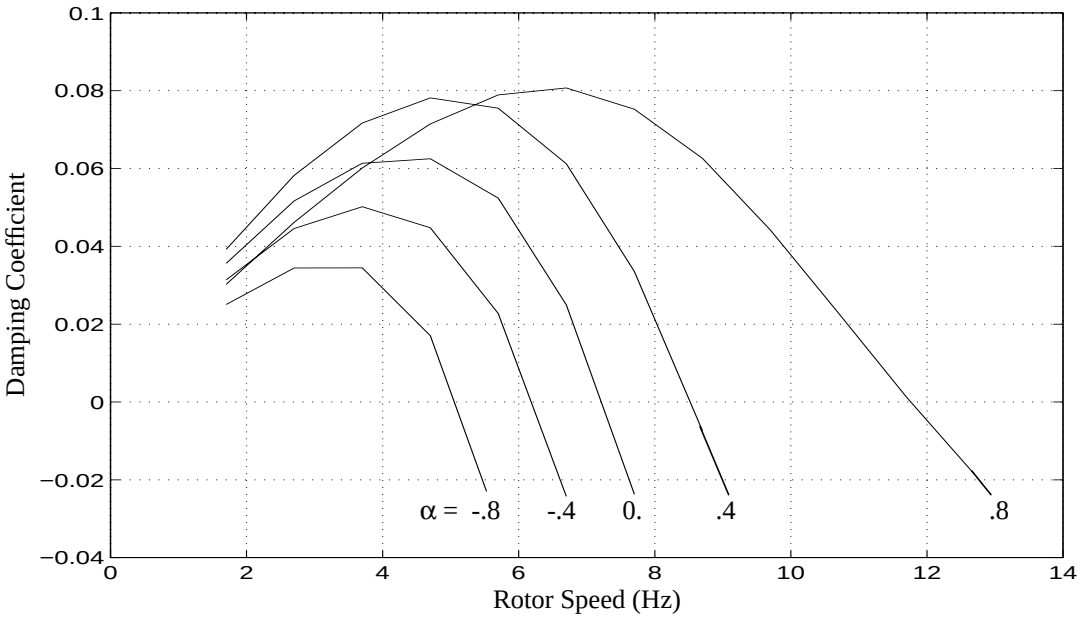

Figure 7. Damping Coefficient for the 1st Torsional Mode of the Bending-Twist Coupled CEB.

problem. As indicated, the effect is symmetric with α, and as the magnitude of α increases the frequencies of the two modes tend toward each other which is generally considered to be destabilizing.

To investigate the coupled behavior of softer blades, a simplified version of Equation 6 can be obtained. For the case of $M_t = 0$ (a reasonable approximation), the following equation relating the rate of change of twist with length to the curvature of the blade is obtained:

$$\frac{\partial \varphi}{\partial x} = \alpha\left(\frac{EI}{GK}\right)^{1/2}\frac{\partial \theta}{\partial x} \qquad (10)$$

A blade with a given cross section can be softened by simply reducing Young's Modulus, in which case the square root term will remain unchanged. However, for the same loading the curvature of the blade will be greater because of the softer material, and the twist per unit length will also be proportionately greater.

Aeroelastic Stability Results

As discussed in the introduction, this investigation of aeroelastic stability is based on the classical theory developed by Theodorsen[11]. These computations include the effects of centrifugal stiffening, rotational coordinate system effects (i.e. Coriolis forces, etc.), and the "tennis racket" effect, in addition to the aeroelasticity and coupling terms that are required for the analysis. In general for aeroelastic stability analyses the airflow is increased until the instability point is reached. For HAWTs the airflow is made up of a component due to the rotation of the rotor and a component due to the ambient wind. In this analysis the component due to the ambient wind is neglected (i.e. the rotor is assumed to be turning in still air) and therefor the rotor speed is simply increased until the system becomes unstable. The remander of this section will address the aeroelastic stability for bending-twist coupling only.

Analyses are completed for both divergence and classical flutter as a function of the coupling coefficient, α. For flutter, the damping coefficient for the first torsional mode (the first mode to go unstable) of the blade is shown in Figure 7 as a function of rotor speed. The various curves correspond to different values of the coupling coefficient. All of the curves show the characteristic increase in the damping coefficient with rotor speed before they fall off to negative values which indicate instability. The critical rotor speed (where the damping coefficient curve crosses the axis) appears to be monotonic with coupling coefficient in a manner similar to swept aircraft wings wherein the sweptback wing, which pitches down as it bends upward, is less stable in flutter, and conversely the sweptforward wing, which pitches up as it bends upward, is more stable. Incidentally, for this vibrational mode, damping coefficients near the operating speed (1.2 Hz.) are larger for the smaller magnitude coupling coefficients (α equal to -.4 and .4 in Figure 7) smaller the extreme coupling coefficients (α equal to -.8 and .8), an undesirable characteristic for load reduction.

These critical rotor speeds are plotted in Figure 8 along

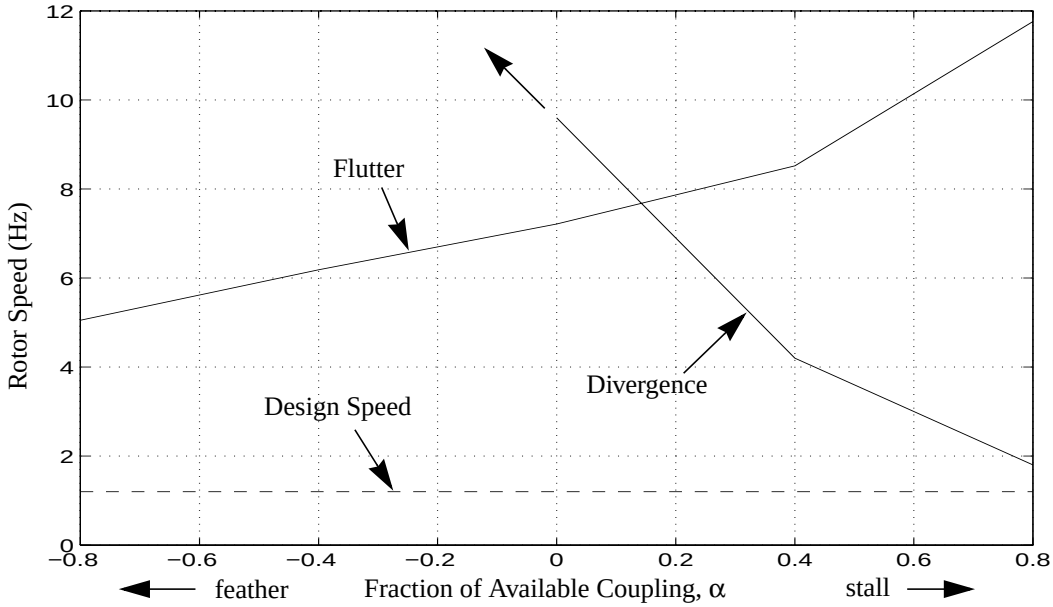

Figure 8. Aeroelastic Stability Boundaries for the Bending-Twist Coupled CEB.

with the divergence rotor speeds as a function of the coupling coefficient. As expected, divergence occurs at lower rotor speeds as the coupling coefficient increases. For positive α, as the blade bends downwind it also twists toward stall, increasing angle of attack and therefor the aeroloads. Conversely for negative α, the blade twists toward feather reducing the aeroloads. In fact as α becomes more negative it is increasingly difficult to get the blade to diverge. For this particular blade the area below the combined flutter and divergence curves represents the region of aeroelastic stability. The horizontal dashed line is the rotor design speed. The blade appears to be less stable at the extreme values of the coupling coefficient and particularly as the blade twists toward stall.

Conclusions and Recommendations

In the development of the coupled elements, limits on the amount of coupling are required to preserve the positive definiteness of the system. These limits are established for both the extension-twist and bending-twist beam elements. For the CEB with the bending-twist coupling these limits proved not to be overly restrictive in that the blade tip twist ranged from $-3°$ to $10°$ for the coupling coefficient varying from -0.8 to 0.8, under loading from the blade rotating at its design speed. Of course there will be practical limits that might be more restrictive than these theoretical ones. For the extension-twist coupling the theoretical limits proved to be much more severe, with tip twist ranging from $0.1°$ to $1.0°$ for the coupling coefficient range noted above.

The aeroelastic instabilities investigated for the bending-twist coupled blade were divergence and classical flutter which are based on linear aerodynamic theory (i.e. blade stall is not considered). Results indicate that this CEB blade is less stable as the extreme values of the coupling coefficient are approached. For blades that twist toward stall ($\alpha > 0$) the instability is driven by divergence, and for twist toward feather ($\alpha < 0$), by flutter, the divergence end of the spectrum being significantly more critical than flutter end. Over the range of coupling coefficients examined, the critical rotor speeds were always above the rotor's design speed.

Recommendations for further work include completing the aeroelastic stability analysis for the case of extension-twist coupling for variable speed applications, completing a parameter study to obtain optimal levels of aerodynamic damping for transient load reduction, fabricating test articles to examine the practical limits of bending-twist coupling and initiating an effort to investigate stall flutter instability for coupled blades that are designed to twist toward stall. Additionally, it is recommended that the ability of these coupled blades to alleviate transient loading without seriously compromising performance be studied, this in an effort to increase fatigue life.

References

1. Karaolis, N. M., G Jeronimidis and P. J. Musgrove, "Composite Wind Turbine Blades: Coupling Effects and Rotor Aerodynamic Performance," EWEC'89, European Wind Energy Conf. Glasgow,

July 10-13, 1989.

2. Karaolis, N. M., P. J. Musgrove and G Jeronimidis, “Active and Passive Aerodynamic Power Control using Asymmetric Fibre Reinforced Laminates for Wind Turbine Blades,” Proc., 10th British Wind Energy Association Conf., D. J. Milbrow Ed., London, March 22-24, 1988.

3. Joosse, P. A. and R. M. van den Berg, “Development of a TenTorTube for Blade Tip Mechanisms, Part 1: Feasibility and Material Tests,” Proc., European Union Wind Energy Conf. and Exhib., GF6teborg, May 20-24, 1996.

4. van den Berg, R. M., P. A. Joosse, and B. J. C. Visser, “Passive Power Control by Self Twisting Blades,” Proc., European Wind Energy Association Conf. and Exhib., Thessaloniki, Oct. 10-14, 1994.

5. Infield D. G. and J. B. Feuchtwang, “Design criteria for passive pitch control of wind turbines using self-twisting blades,” International Journal of Ambient Energy, Vol. 16, No. 3, July 1995.

6. Feuchtwang, J. B. and D. G. Infield, “Aerofoil profile section for passive pitch control using self-twisting blades,” Wind Energy Conversion, Proc. 17th BWEA Wind Energy Conf., ed. J. Halliday, BWEA, Warwick, July 19-21, 1995.

7. Lobitz, D. W., P. S. Veers and P. G. Migliore, “Enhanced Performance of HAWTs Using Adaptive Blades,” Proc. Wind Energy ‘96, ASME Wind Energy Symposium, Houston, Jan. 29 - Feb. 2, 1996.

8. Corbet, D. C. and C. A. Morgan, “Report on the Passive Control of Horizontal Axis Wind Turbines,” ETSU WN 6043 report by Garrad, Hassan and Partners, Bristol, UK, 1992.

9. Eggers, A. J., H. Ashley, S. M. Rock, K. Cheney, and R. Digumarthi, “Effects of Blade Bending on Aerodynamic Control of Fluctuating Loads on Teetered HAWT Rotors,” Journal of Solar Energy Engineering, Trans. of the ASME, Vol. 118, No. 4, Nov. 1996.

10. D. W. Lobitz, “A NASTRAN-Based Computer Program for Structural Dynamic Analysis of Horizontal Axis Wind Turbines,” Proceedings of the Horizontal Axis Wind Turbine Technology Workshop, Department of Energy and NASA-Lewis, Cleveland, May 1984.

11. R. L. Bisplinghoff, H. Ashley and R. L. Halfman, Aeroelasticity, Addison-Wesley Publishing Company, 1955, p.272.

12. D. W. Lobitz and T. D. Ashwill, “Aeroelastic Effects in the Structural Dynamic Analysis of Vertical Axis Wind Turbines,” Proceedings of the Windpower 85 Conference, San Francisco, August 1985.